ADVANCES IN ATMOSPHERIC SCIENCES, VOL. 41, SEPTEMBER 2024, 1691–1703

• **Original Paper** •

Different ENSO Impacts on Eastern China Precipitation Patterns in Early and Late Winter Associated with Seasonally-Varying Kuroshio Anticyclonic Anomalies

Jingrui YAN, Wenjun ZHANG*, Suqiong HU, and Feng JIANG

Key Laboratory of Meteorological Disaster, Ministry of Education (KLME)/Joint International Research Laboratory of Climate and Environment Change (ILCEC)/Collaborative Innovation Center on Forecast and Evaluation of Meteorological Disasters (CIC-FEMD), Nanjing University of Information Science and Technology, Nanjing 210044, *China*

(Received 24 August 2023; revised 14 December 2023; accepted 4 January 2024)

ABSTRACT

Winter precipitation over eastern China displays remarkable interannual variability, which has been suggested to be closely related to El Niño–Southern Oscillation (ENSO). This study finds that ENSO impacts on eastern China precipitation patterns exhibit obvious differences in early (November–December) and late (January–February) winter. In early winter, precipitation anomalies associated with ENSO are characterized by a monopole spatial distribution over eastern China. In contrast, the precipitation anomaly pattern in late winter remarkably changes, manifesting as a dipole spatial distribution. The noteworthy change in precipitation responses from early to late winter can be largely attributed to the seasonally varying Kuroshio anticyclonic anomalies. During the early winter of El Niño years, anticyclonic circulation anomalies appear both over the Philippine Sea and Kuroshio region, enhancing water vapor transport to the entirety of eastern China, thus contributing to more precipitation there. During the late winter of El Niño years, the anticyclone over the Philippine Sea is further strengthened, while the one over the Kuroshio dissipates, which could result in differing water vapor transport between northern and southern parts of eastern China and thus a dipole precipitation distribution. Roughly the opposite anomalies of circulation and precipitation are displayed during La Niña winters. Further analysis suggests that the seasonally-varying Kuroshio anticyclonic anomalies are possibly related to the enhancement of ENSO-related tropical central-eastern Pacific convection from early to late winter. These results have important implications for the seasonal-to-interannual predictability of winter precipitation over eastern China.

Key words: precipitation, eastern China, ENSO, early winter, late winter, Kuroshio anticyclone

Citation: Yan, J. R., W. J. Zhang, S. Q. Hu, and F. Jiang, 2024: Different ENSO impacts on eastern China precipitation patterns in early and late winter associated with seasonally-varying Kuroshio anticyclonic anomalies. *Adv. Atmos. Sci.*, **41**(9), 1691−1703, https://doi.org/10.1007/s00376-023-3196-1.

Article Highlights:

- ENSO-associated precipitation anomalies exhibit different spatial patterns over eastern China in early and late winter. A monopole precipitation anomaly pattern is detected in early winter while the precipitation anomaly in late winter is characterized by a meridional dipole spatial distribution.
- The remarkable change in precipitation responses to ENSO from early to late winter can be largely attributed to the seasonally-varying Kuroshio anticyclonic anomalies, possibly due to the enhancement of ENSO-associated tropical central-eastern Pacific convection from early to late winter.

1. Introduction

As the strongest signal of interannual variability in the climate system, El Niño–Southern Oscillation (ENSO) is an important source of seasonal-to-interannual climate predictability (Wallace et al., 1998; McPhaden et al., 2006). Although ENSO originates and develops mainly in the tropical Pacific, it can lead to large-scale atmospheric circulation anomalies around the globe and thus regional weather and climate anomalies through so-called atmospheric teleconnections (Ropelewski and Halpert, 1987; Trenberth and Caron, 2000; Alexander and Scott, 2002). For instance, ENSO exerts a substantial impact on the North Pacific–North Ameri-

* Corresponding author: Wenjun ZHANG
Email: zhangwj@nuist.edu.cn

© Institute of Atmospheric Physics/Chinese Academy of Sciences, and Science Press 2024

can climate via Pacific–North America (PNA) teleconnection (Hoskins and Karoly, 1981; Wallace and Gutzler, 1981). ENSO affects the climate variability over the North Atlantic–European sector through the North Atlantic Oscillation (NAO) (Moron and Gouirand, 2003; Brönnimann, 2007; Ineson and Scaife, 2009).

ENSO also exerts a substantial influence on the East Asian climate by modifying the low-level anticyclonic circulation over the western North Pacific (WNP) region (e.g., Zhang et al., 1996, 2017; Wang et al., 2000; Yang et al., 2007; Xie et al., 2009). The anomalous WNP anticyclone usually establishes itself in the boreal autumn of the ENSO developing year, peaking in the spring of the decaying year and lasting until summer (e.g., Harrison and Larkin, 1996; Wang et al., 2000). It has been well established that winter precipitation over eastern China exhibits notable interannual variations, which is suggested to be closely related to ENSO (e.g., Li and Ma, 2012; Zhang et al., 2015b, 2016; Geng et al., 2021). During winters with a mature El Niño, the southwesterly wind anomalies located in the northwestern flank of the anomalous WNP anticyclone tend to weaken climatological northeasterly winds and enhance water vapor transport towards eastern China, leading to increased precipitation over eastern China; while La Niña winters present nearly opposite effects (e.g., Wu et al., 2003; Zhou and Wu, 2010; Yuan and Yang, 2012). Several studies pointed out that ENSO exerts complicated impacts on winter precipitation over eastern China. For example, significantly positive precipitation anomalies cover southern China during El Niño winters, while only weak precipitation anomalies can be observed during La Niña winters (e.g., Wu et al., 2010; Zhang et al., 2015a; Guo et al., 2017). In recent decades, a new type of El Niño has been frequently observed with its center of action in the Central Pacific (CP), which differs considerably from the traditional El Niño that features its sea surface temperature (SST) anomaly centered in the Eastern Pacific (EP) (Larkin and Harrison, 2005; Ashok et al., 2007; Weng et al., 2007; Kao and Yu, 2009; Kug et al., 2009; Ren and Jin, 2011). These two types of ENSO events exhibit different impacts on winter precipitation in Eastern China (Su et al., 2010; Xu et al., 2019). Specifically, during EP El Niño winters, southern China experiences positive precipitation anomalies (Feng et al., 2010; Xu et al., 2019). In contrast, there is a decrease in precipitation over the same region during CP El Niño winters (Su et al., 2013; Li et al., 2018).

Previous studies have shown that the ENSO atmospheric responses over many regions exhibit obvious sub-seasonal variations (Livezey et al., 1997; Mariotti et al., 2002; Moron and Gouirand, 2003; Gill et al., 2015); therefore, conventional winter-mean analyses (December–February or December–March) may obscure sub-seasonal features of ENSO atmospheric teleconnections (Bladé et al., 2008; Kim et al., 2018). For example, during the 2015/16 super El Niño winter, it was expected that the anomalous low-level anticyclone over the WNP should have resulted in the more frequent northward transport of moist and warm air masses into East Asia, thus leading to winter conditions that were warmer and wetter than normal. However, there were no obvious temperature anomalies observed over East Asia during the 2015/16 boreal winter, due to the obvious sub-seasonal variation in temperature with warm anomalies in early winter and cold anomalies in late winter (Geng et al., 2017). This raises the question of whether the impacts of ENSO on winter precipitation anomalies over eastern China have similar sub-seasonal differences. Understanding the sub-seasonal variations of precipitation over eastern China during ENSO winters has important implications for improving East Asian climate prediction. In this work, different precipitation spatial distributions are present over eastern China in ENSO early and late winter. This sub-seasonal variation can be largely attributed to the seasonally-varying Kuroshio anticyclonic pressure anomalies, possibly due to the enhancement of ENSO-associated convection over the tropical central and eastern Pacific from early to late winter.

The remainder of this paper is organized as follows. Section 2 introduces the data and methodology used. Section 3 presents the differences in ENSO impacts on precipitation over eastern China in early and late winter. Possible physical mechanisms are investigated in section 4. In section 5, we further verify our observed results based on model simulations. Finally, a summary and discussion are provided in section 6.

2. Data and methods

The datasets used in this work include (1) monthly mean SST data on a 1° × 1° grid from the Met Office Hadley Centre (Rayner et al., 2003); (2) monthly mean precipitation data from the Climate Prediction Center Merged Analysis of Precipitation (CMAP) (Xie and Arkin, 1997), with a horizontal resolution of 2.5° × 2.5°; (3) monthly mean atmosphere data from the fifth generation of the European Center for Medium-Range Weather Forecast (ECMWF) atmospheric reanalysis (ERA5) dataset (Hersbach et al., 2020). The reanalysis data employed includes the monthly mean zonal (u) and meridional (v) wind, sea level pressure (SLP), 300-hPa geopotential height (H), and the specific humidity across 20 vertical levels from 1000 to 300 hPa, with a horizontal resolution of 0.25° × 0.25°. In addition, we examine ENSO impacts on precipitation and atmospheric circulation anomalies in 28 atmospheric general circulation models [AGCMs, Table S1 in the electronic supplementary material (ESM)], forced by the Atmospheric Model Inter-comparison Project, version 6 (AMIP6)-style SST boundary conditions from 1979 to 2014 (Eyring et al., 2016). The simulation results from the first ensemble member (r1i1p1f1) for each model are utilized. All model data are bi-linearly interpolated into a common horizontal grid of 2.5° × 2.5° for comparison with the reanalysis data (Kirkland, 2010). Our analyses span 1980–2020, and anomalies for all variables are obtained by removing the monthly mean climatology over the entire study period. The low-frequency components are suppressed by performing an 8-year highpass Lanczos filter to focus on

the interannual variability (Duchon, 1979).

The Niño-3.4 index (SST anomalies in the region of 5°S–5°N, 120°–170°W) is used to represent the ENSO variability. Thirteen El Niño and fourteen La Niña winters over the period 1980–2020 are identified by the Climate Prediction Center (CPC) based on a threshold of ±0.5 standard deviations of the Niño-3.4 index (Table 1). The year listed in Table 1 corresponds to year(0)/year(1), where 0 and 1 stand for the developing and decaying years of ENSO events, respectively. Two precipitation indices are defined based on the regressed precipitation anomaly patterns on early winter and late winter Niño-3.4 indices. The monopole precipitation index (MPI) is calculated as the standardized area-averaged precipitation anomalies in the region bounded by 23°–42°N 105°–123°E. The dipole precipitation index (DPI) is calculated as the difference of the standardized precipitation anomalies between the northern (31°–39°N, 105°–113°E) and southern (23°–31°N, 107°–123°E) regions of eastern China. Based on the regressed SLP anomalies onto the Niño-3.4 index, the Kuroshio index is defined as the standardized area-averaged SLP anomalies over the Kuroshio region (35°–50°N, 135°–165°E), the Philippines index is defined as the standardized area-averaged SLP anomalies over the Philippines region (0°–20°N, 120°–143°E), and the Aleutian index is defined as the standardized area-averaged SLP anomalies over the Aleutian region (35°–60°N, 180°–135°W). In this study, the boreal winter is divided into early winter (November–December, ND) and late winter (January–February, JF). All statistical significance tests are inferred using a two-tailed Student's *t*-test.

3. Different ENSO impacts on the precipitation pattern over eastern China in early and late winter

Figure 1 displays the spatial distribution of precipitation climatology and variance over eastern China in early and late winter. Climatological precipitation maxima are mainly concentrated over southern China both in early and late winter, with the precipitation amount in late winter larger than that in early winter by about 1 mm d^{-1}. Consistent with the spatial distribution of climatological precipitation, the precipitation variability over southern China is much greater than that in other regions both in early and late winter except that the maximum variability center in late winter moves southward of 25°N. To explore the different impacts of ENSO on precipitation anomalies over eastern China in early and late winter, Figs. 2a–c display regressed precipitation anomalies onto the simultaneous Niño-3.4 index during the entire win-

Table 1. El Niño and La Niña winters.

El Niño	1982/1983, 1986/1987, 1987/1988, 1991/1992, 1994/1995, 1997/1998, 2002/2003, 2004/2005, 2006/2007, 2009/2010, 2014/2015, 2015/2016, 2018/2019
La Niña	1983/1984, 1984/1985, 1988/1989, 1995/1996, 1998/1999, 1999/2000, 2000/2001, 2005/2006, 2007/2008, 2008/2009, 2010/2011, 2011/2012, 2016/2017, 2017/2018

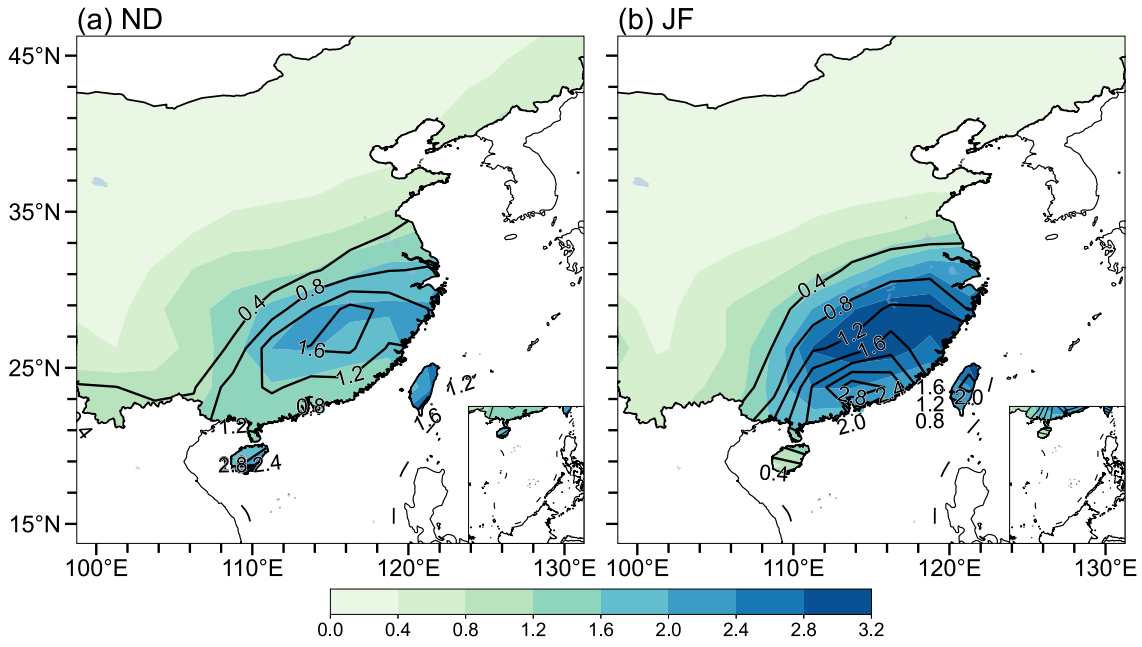

Fig. 1. (a) Climatology (shading; mm d^{-1}) and variance (contour; mm^2 d^{-2}) of early winter precipitation. (b) Same as (a), but for the late winter.

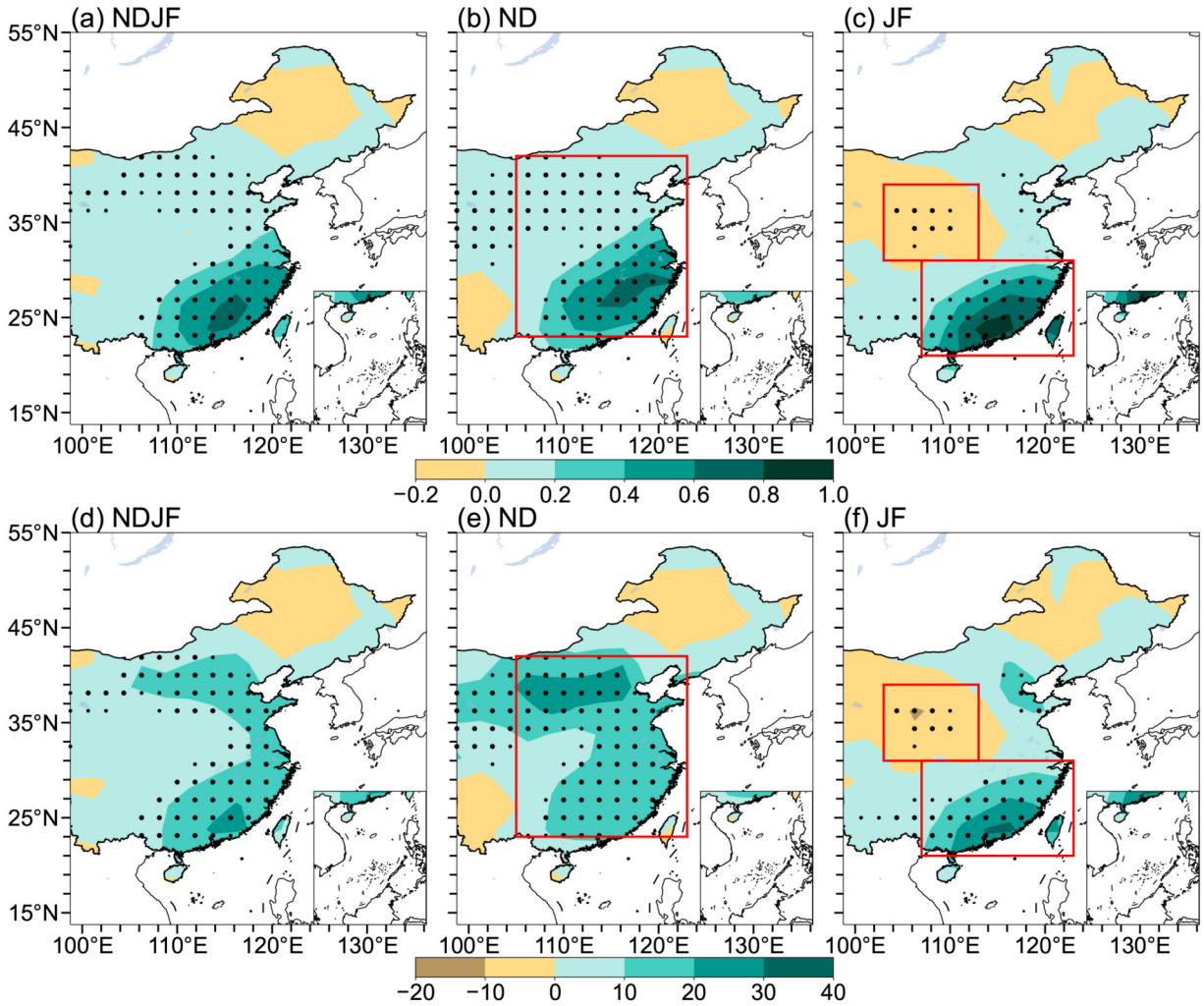

Fig. 2. Precipitation anomalies (shading; mm d^{-1}) regressed onto the simultaneous Niño-3.4 index for the (a) entire winter, (b) early winter, and (c) late winter. (d–f) Similar to (a–c), but for the percentage of precipitation anomaly (shading; %). The small and big black dots indicate the values exceeding the 90% and 95% confidence levels, respectively. The red boxes in (b) and (e) are used to calculate the MPI, while the red boxes in (c) and (f) are used to calculate the DPI.

ter, early winter, and late winter. For the entire winter mean (Fig. 2a), ENSO-related precipitation anomalies exhibit a monopole spatial distribution over eastern China, with positive (negative) precipitation anomalies during El Niño (La Niña) years. The precipitation anomaly pattern in early winter also manifests as a monopole distribution (Fig. 2b), similar to that in the entire winter. In contrast, ENSO-related precipitation anomalies in late winter exhibit a meridional dipole pattern with positive anomalies over southern China and negative anomalies over central China (Fig. 2c). Considering that the spatial distribution of climatological precipitation is extremely uneven across eastern China (Fig. 1a), we further show the percentages of precipitation anomalies regressed onto the Niño-3.4 index (Figs. 2d–f). The percentage of precipitation anomaly represents the ratio of the precipitation anomaly to the climatological precipitation. Similarly, a monopole spatial distribution exists over eastern China in early winter, while precipitation anomalies in late winter feature a dipole spatial distribution.

Here, two precipitation indices are defined to represent the variability of precipitation anomaly associated with ENSO in early and late winter, respectively (see methods; MPI and DPI). The MPI in early winter shows a high correlation with the Niño-3.4 index (R=0.73, statistically significant at a 95% confidence level), while the DPI in late winter exhibits a significant relationship with the Niño-3.4 index (R=0.59, statistically significant at 95% confidence level). Figure 3 further shows the composite difference of precipitation anomalies between El Niño and La Niña events. For the early winter, significantly positive precipitation anomalies cover almost the entirety of eastern China (Fig. 3a), similar to that in Figs. 2b and 2e. In late winter, precipitation anomalies over eastern China show a north-south dipole pattern (Fig. 3b), characterized by positive anomalies over southern China and negative anomalies over central China, similar to those in Figs. 2c and 2f.

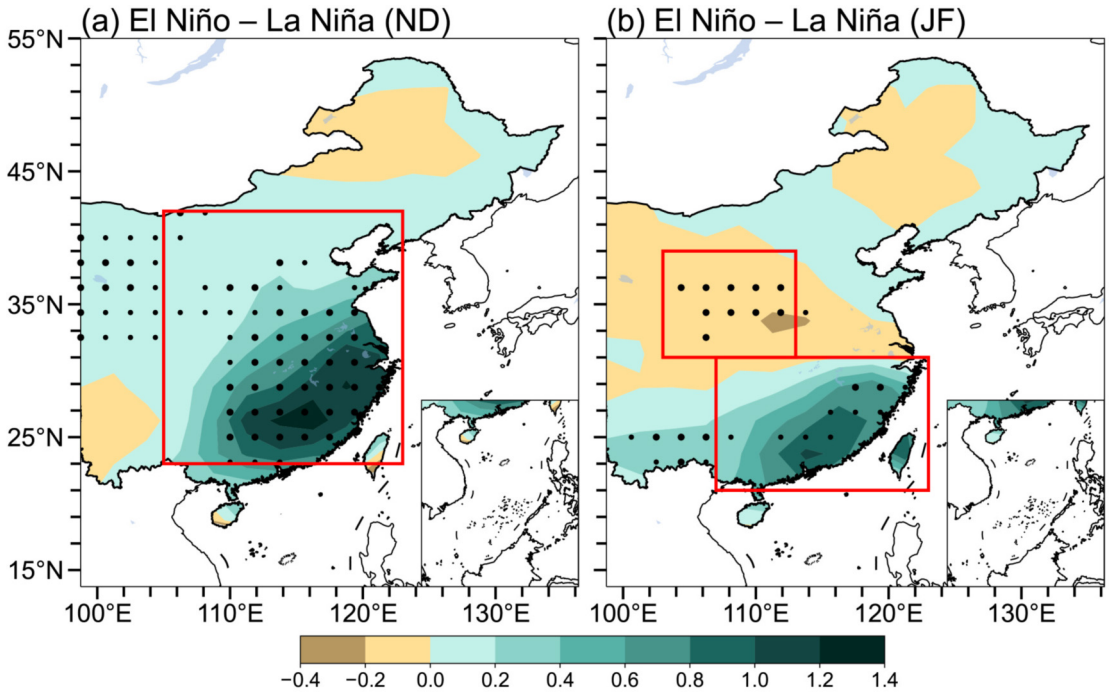

Fig. 3. (a) Composite difference of precipitation anomalies (shading; mm d^{-1}) between El Niño and La Niña years for the early winter. (b) Same as in (a), but for the late winter. The small and big black dots indicate values exceeding the 90% and 95% confidence levels, respectively. The red boxes in (a) and (b) are used to calculate the MPI and DPI, respectively.

4. Possible mechanisms for different ENSO impacts on early and late winter precipitation patterns

Previous studies revealed that the physical mechanism by which ENSO affects winter precipitation is through the modulation of the large-scale atmospheric circulations and thus the local water vapor transport (Zhang and Sumi, 2002; Zhou and Wu, 2010; Yin and Wang, 2016; He et al., 2019). Figure 4 compares the ENSO-associated water vapor transport anomalies in early and late winter. For early winter, significant northward water vapor flux anomalies cover the entirety of eastern China, which can transport warm and moist airflow from the South China Sea and the Bay of Bengal, a pattern conducive to the increased precipitation (Fig. 4a). However, in late winter, northward water vapor flux anomalies are limited to the southern part of eastern China. Over the northern part of eastern China, there are southward water vapor flux anomalies; thus, the warm and moist water vapor over oceans cannot be transported into northern China (Fig. 4b). This could lead to a meridional dipole pattern of precipitation anomaly over eastern China in late winter.

Figure 5 displays the ENSO-related atmospheric circulation anomalies at different levels during early and late winter. During El Niño early winter, significant anticyclonic anomalies can be detected over the WNP at low levels (850 hPa), with two action centers, located over the Philippine Sea and the Kuroshio region (Fig. 5a). The combination of these two anticyclonic anomalies results in significant southerly anomalies over entirety of eastern China, contributing to a monopole precipitation anomaly pattern in early winter. In contrast, the anticyclonic circulation located over the Kuroshio region disappears in late winter, occurring in tandem with the further development of the Philippine anticyclone (Fig. 5b), a pattern transition that could lead to the southerly water vapor transport confined in southeastern China and a dipole precipitation pattern in late winter. At 300 hPa (Figs. 5c, d), the low-level circulation over the Philippine Sea exhibits an opposite anomaly to that at high levels, due to the baroclinic characteristics inherent in the tropical atmosphere. However, corresponding to the equivalent barotropic structure in the mid-to-high latitude atmosphere, the sub-seasonal change in the Kuroshio atmospheric circulation anomalies at 300 hPa is similar to that at 850 hPa. To better illustrate the changes in the Kuroshio and Philippine anticyclones from early to late winter, Fig. 6 displays the composite differences of Kuroshio and Philippines anticyclone indices between El Niño and La Niña years for the early and late winter periods. It is clear that the Kuroshio anticyclone dissipates and the Philippine anticyclone further strengthens during the transition from early to late winter.

The possible reason for the disappearance of the Kuroshio anticyclone in late winter is worthy of further attention. Considering that tropical heating is a more direct factor in forcing atmospheric teleconnections (e.g., Chiodi and Harrison, 2013, 2015; Cai et al., 2014), Fig. 7 compares the tropical precipitation anomalies related to ENSO in early and late winter when significantly positive and negative precipitation

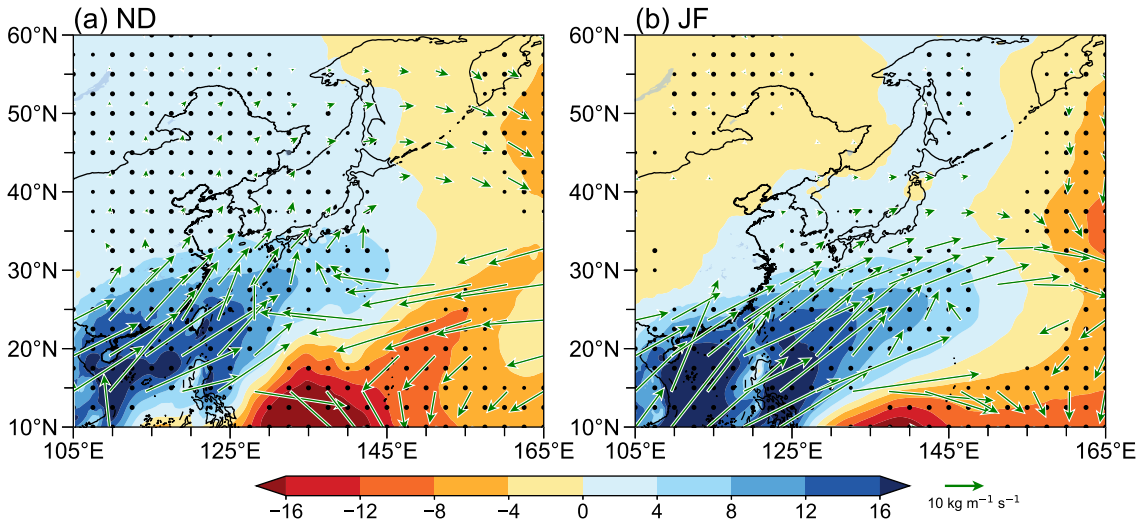

Fig. 4. (a) Regressed vertically integrated water vapor flux anomalies (vectors; kg m^{-1} s^{-1}) and its meridional component on the early winter Niño-3.4 index (shading; kg m^{-1} s^{-1}). (b) Same as in (a), but for the late winter. The small and big black dots indicate the values exceeding the 90% and 95% confidence levels, respectively. The flux anomalies are shown only when their significance meets or exceeds the 90% confidence level.

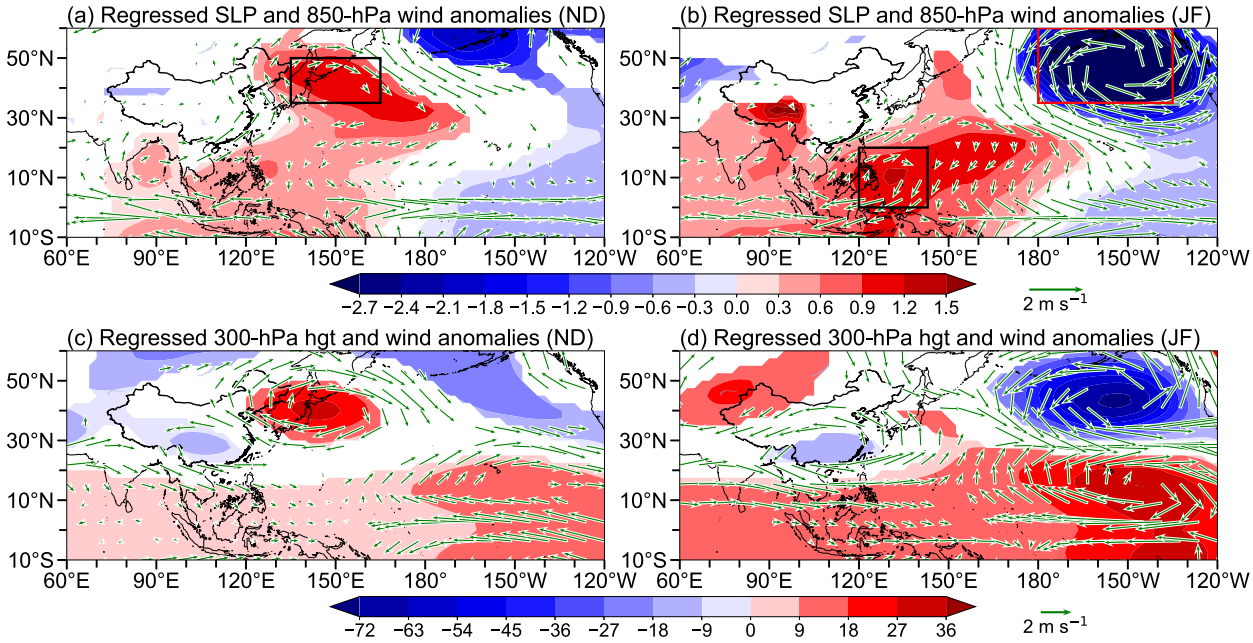

Fig. 5. Regressed SLP (shading; hPa) and 850-hPa wind (vector; m s^{-1}) anomalies onto the Niño-3.4 index for the (a) early winter and (b) late winter. (c, d) Similar to (a, b), but for the 300-hPa geopotential height (shading; m) and wind (vector; m s^{-1}) anomalies. The black box in (a) is used to calculate the Kuroshio index, while the black and red boxes in (b) are used to calculate the Philippines and Aleutian indices, respectively. Only the SLP, geopotential height, and wind anomalies with statistical significance that meet or exceed the 90% confidence level are shown.

anomalies occur in the tropical central-eastern and western Pacific, respectively—a typical ENSO-associated dipole precipitation pattern (Figs. 7a, b). Figure 7c further displays the regressed differences in precipitation anomalies between the early and late winter on the winter Niño-3.4 index. It shows that the tropical central-eastern Pacific convection is significantly enhanced and the tropical western Indian Ocean convection weakens in late winter. Previous studies have shown that the sub-seasonal enhancement of the tropical Pacific convection could lead to a notable strengthening of the Aleutian Low anomalies over the North Pacific (e.g., Bladé et al., 2008; Son et al., 2014; Kim et al., 2018; Hu et al., 2023). As displayed in Figs. 5 and 6, the Aleutian Low exhibits a sub-seasonal enhancement from early to late winter of ENSO years. The remarkable enhancement of the Aleutian Low response in late winter could suppress the anticyclone over the Kuroshio region, which may be responsible for the disappearance of the Kuroshio anticyclonic anomalies. Some previ-

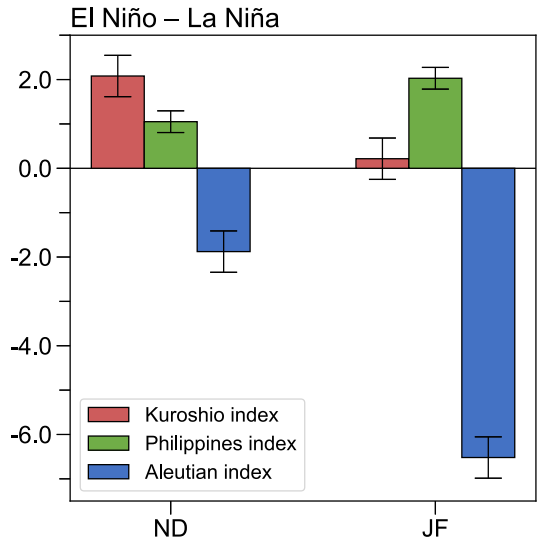

Fig. 6. Composite differences of Kuroshio (red bars), Philippines (green bars), and Aleutian indices (blue bars) between El Niño and La Niña years for the early and late winter, with error bars of one standard deviation.

ous studies also suggest that convection anomalies in the tropical Indian Ocean also play a role in the ENSO atmospheric teleconnection in early winter (Ma et al., 2022; Park et al., 2023).

5. Impacts of ENSO on early and late precipitation anomaly patterns over eastern China in AMIP6 simulations

To substantiate the observed results, we further examine the impacts of ENSO on early and late winter precipitation over eastern China in AMIP6 simulations. The simulations are conducted with prescribed observed SST and sea ice data, which can extend our investigation beyond the limited observational record. Figure S1 (in the ESM) displays the regressed precipitation anomalies over southern China onto the winter Niño-3.4 index in 28 AMIP6 models. It shows that 12 models could simulate significantly positive precipitation anomalies similar to those in observations. ENSO-related impacts on early and late winter precipitation are further examined in these 12 models, and 7 of 12 models are

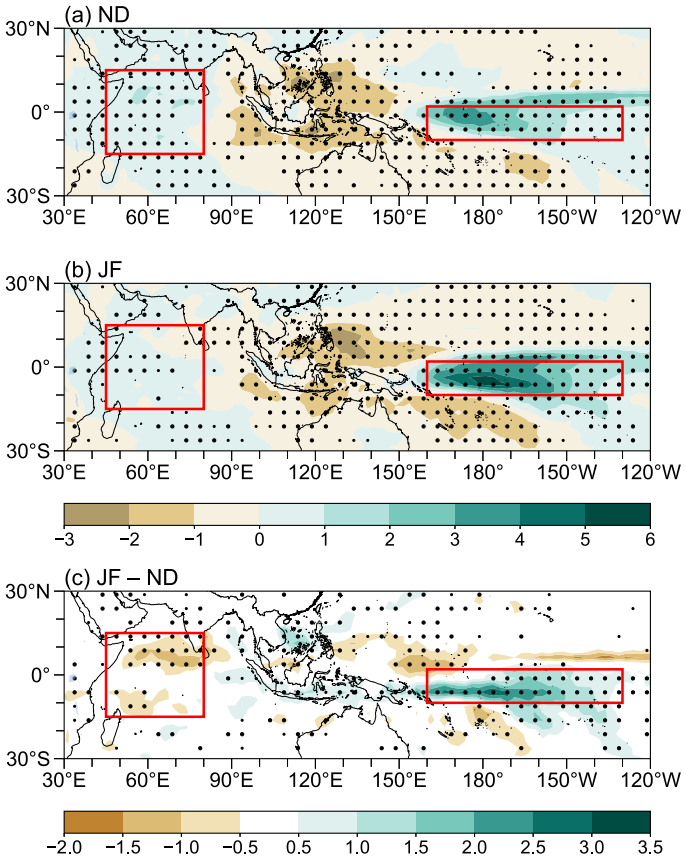

Fig. 7. (a) Regressed tropical precipitation anomalies (shading; mm d^{-1}) onto the winter Niño-3.4 in the early winter. (b) Same as in (a), but for the late winter. (c) Differences in the regressed tropical precipitation anomalies (shading; mm d^{-1}) between the early and late winter on the winter Niño-3.4 index. The red boxes represent the region of the tropical western Indian Ocean and tropical central-eastern Pacific. The small and big black dots indicate the values exceeding the 90% and 95% confidence levels, respectively.

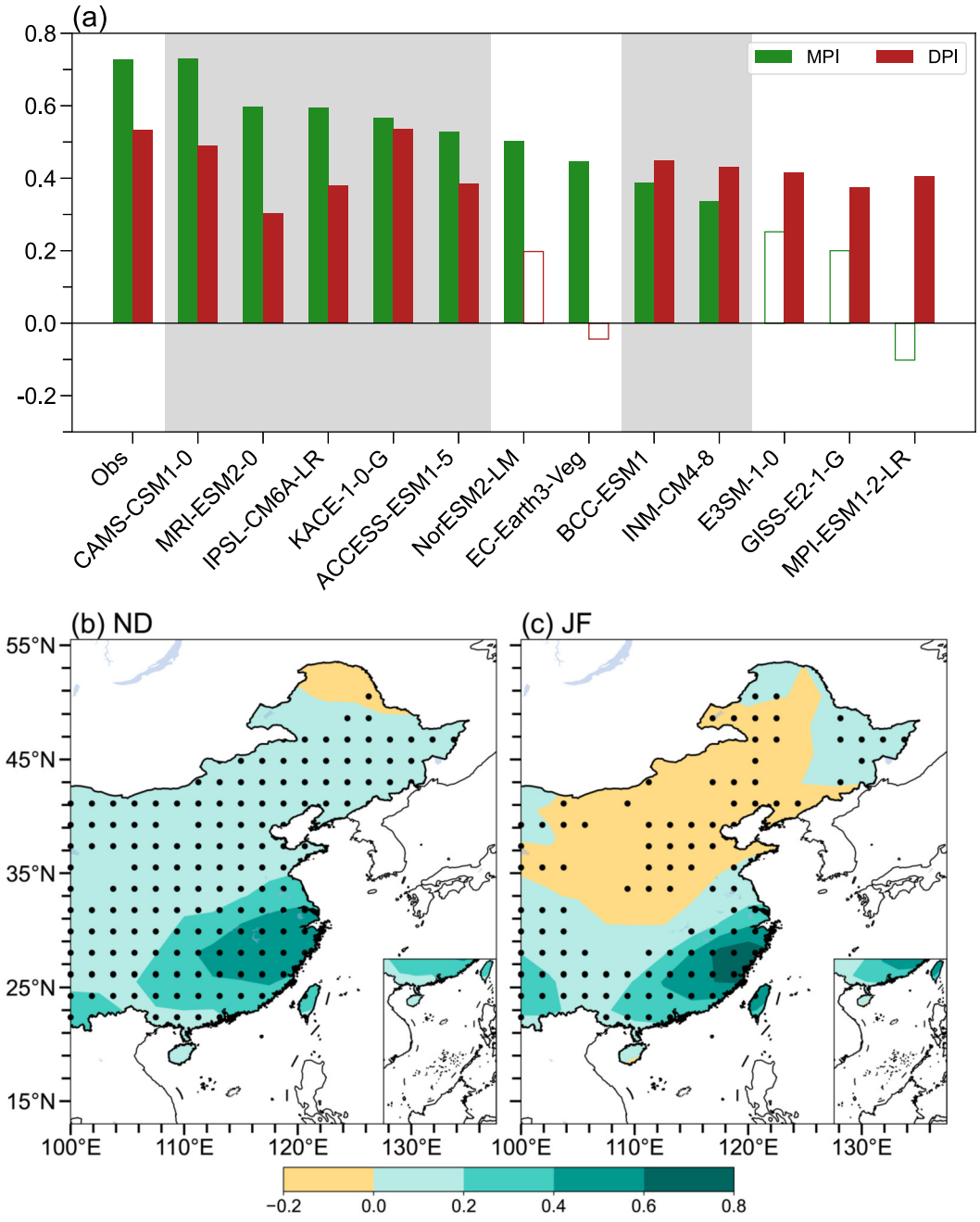

Fig. 8. (a) Regressed MPI (green bars) and DPI (red bars) onto the winter Niño-3.4 index in observations and 12 AMIP6 models. Solid bars represent values that exceed the 95% confidence level. Gray shading indicates the selected 7 models. (b) Simulated precipitation anomalies (shading; mm d^{-1}) regressed onto the early winter Niño-3.4 index. (c) Same as in (b), but for the late winter. Dots denote that at least 5 of 7 models have precipitation anomalies of the same sign.

finally selected since these models could simulate the observed sub-seasonal change from the monopole pattern in early winter to the dipole pattern in late winter (Fig. 8a). Figures 8b and 8c display the regressed precipitation anomalies onto the winter Niño-3.4 index in early and late winter based on the ensemble mean of these selected seven models. Similar to those in observations (Figs. 2b, c), the precipitation anomalies related to ENSO in early winter are characterized by a monopole distribution, while a meridional dipole precipitation pattern appears in late winter.

The simulated change of ENSO-related precipitation anomalies from early to late winter can also be explained by the disappearance of the Kuroshio anticyclone in late winter. As shown in Figs. 9a and 9c, the southerly wind anomalies associated with the Philippines and Kuroshio anticyclones could transport more water vapor into the entirety of eastern China, leading to the monopole pattern of precipitation anomalies. In contrast, the disappearance of the Kuroshio anti-

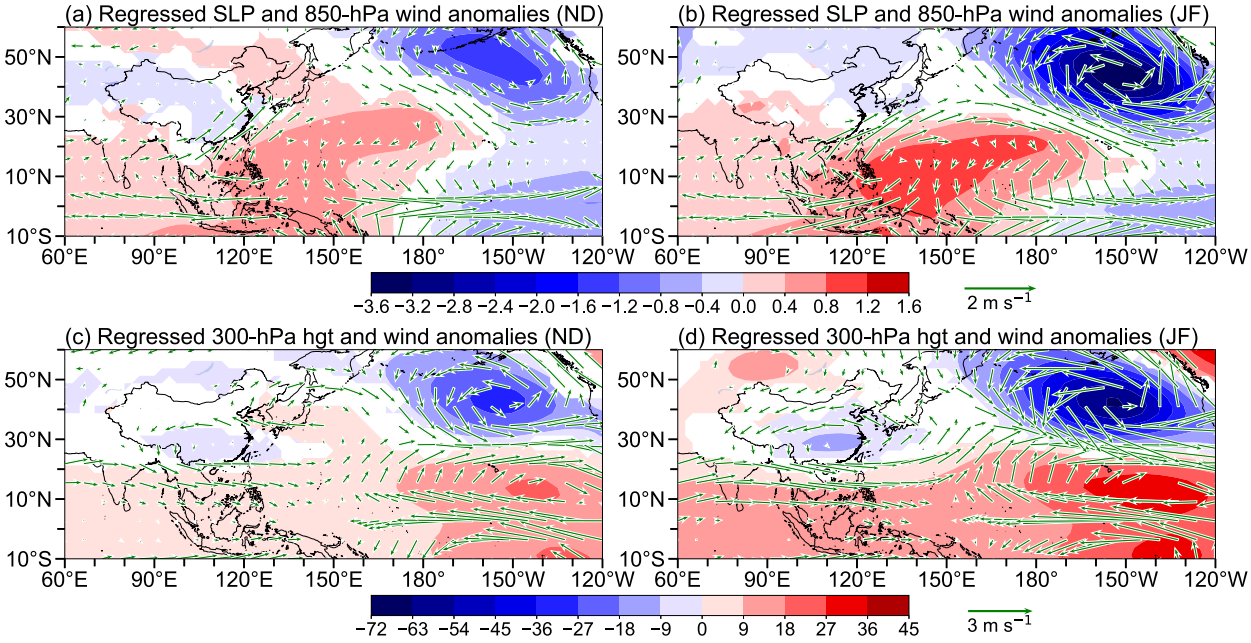

Fig. 9. Simulated SLP (shading; hPa) and 850-hPa wind (vector; m s^{-1}) anomalies regressed onto the Niño-3.4 index for the (a) early winter and (b) late winter. (c) and (d) Similar to (a) and (b), but for geopotential height (shading; m) and wind (vector; m s^{-1}) anomalies at 300 hPa. Shading denotes that 5 models at least of 7 models have in-sign geopotential height and SLP anomalies. Vector denotes that at least 5 out of 7 models have wind anomalies of the same sign.

cyclone in late winter leads to the water vapor transport being confined over southern China and a dipole precipitation pattern (Figs. 9b, and d). Figure 10 further compares the tropical precipitation anomalies related to ENSO in early and late winter. It shows that ENSO-associated precipitation patterns can be well simulated in these models, with increased convection in the tropical central-eastern Pacific and weakened convection in the tropical western Pacific (Figs. 10a, b). The differences in tropical precipitation anomalies between the early and late winter are displayed in Fig. 10c. These models can also reproduce the enhanced tropical central-eastern Pacific precipitation in late winter, although some differences do exist in other tropical regions.

6. Conclusions and discussion

In this study, we investigated different impacts of ENSO on precipitation anomalies over eastern China in early and late winter during 1980–2020. In early winter, ENSO-associated precipitation anomalies over eastern China exhibit a monopole spatial distribution. In contrast, the precipitation anomaly pattern in late winter obviously differs from that in early winter, characterized by a meridional dipole spatial distribution. The remarkable change in precipitation responses from early to late winter is mainly due to the seasonally varying Kuroshio anticyclonic anomalies. In the early winter of El Niño years, anticyclonic circulation anomalies appear both over the Philippine Sea and Kuroshio region, enhancing water vapor transport to the entirety of eastern China, thus contributing to more precipitation there. During the late winter of El Niño years, the anomalous anticyclone over the Philippine Sea is further strengthened, while the one over the Kuroshio dissipates. This results in different water vapor transport anomalies over the northern and southern parts of eastern China, conducive to a dipole precipitation distribution. Roughly opposite anomalies of circulation and precipitation are displayed during La Niña winters. Further analyses suggest that the seasonally-varying Kuroshio anticyclonic anomalies are possibly related to the enhancement of ENSO-related tropical central-eastern Pacific convection from early to late winter. This observed impact of precipitation over eastern China by ENSO is further substantiated by the modeling simulations. Seven models could well reproduce the subseasonal variation of ENSO impact on winter precipitation over eastern China and the seasonally varying Kuroshio anticyclonic anomalies. However, more than half of AMIP6 models exhibit limitations in simulating ENSO-associated atmospheric responses, highlighting the need for ongoing model improvement efforts.

ENSO-associated climate responses are diverse and related to factors such as the zonal location and strength of SST anomalies (e.g., Ashok et al., 2009; Feng et al., 2010; Jiang et al., 2019). Here, it is found that the differences in precipitation anomaly patterns between early and late winter can be obtained both in EP and CP ENSO events although the precipitation anomalies during CP ENSO events are relatively weak compared to those during EP ENSO events (not shown). Notably, some studies pointed out that the climate impacts of CP ENSO events depend on their zonal location. Therefore, future research is needed to fully understand the interannual variability of winter precipitation across eastern China.

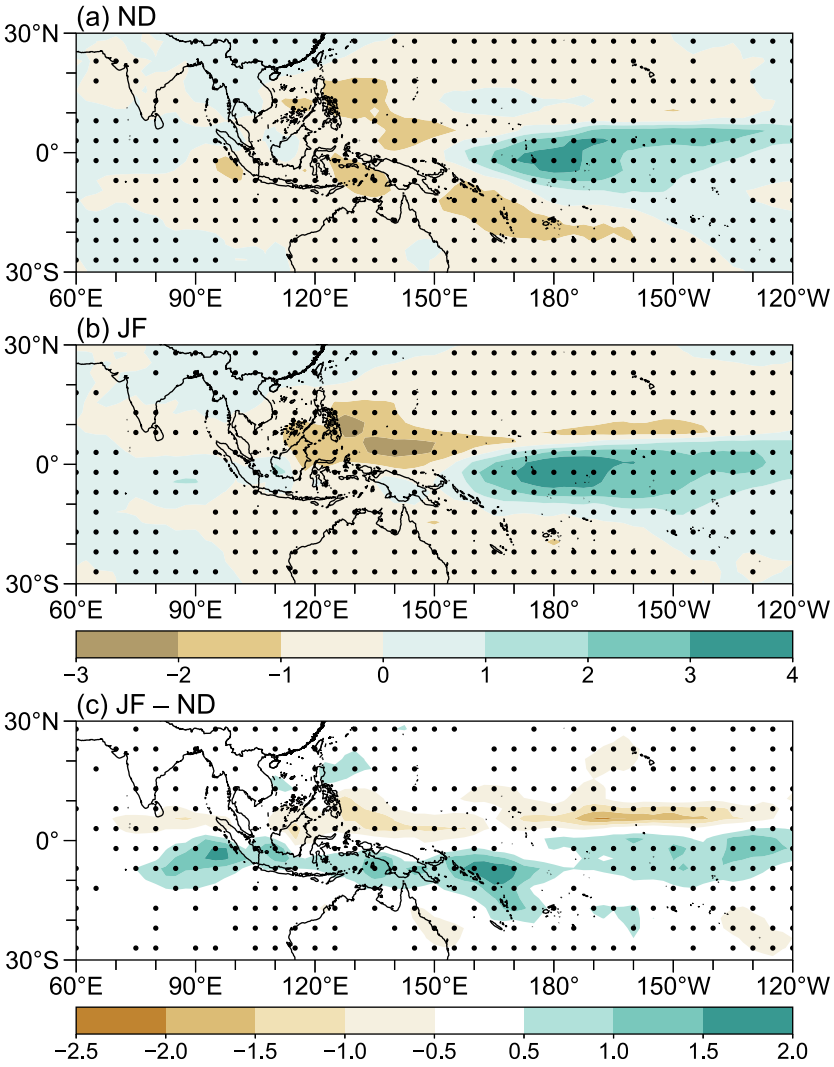

Fig. 10. (a) Simulated tropical precipitation anomalies (shading; mm d^{-1}) regressed onto the winter Niño-3.4 index in early winter. (b) Same as in (a), but for the late winter. (c) Simulated tropical precipitation anomalies differences (shading; mm d^{-1}) between the early and late winter regressed onto winter Niño-3.4. Dots denote that at least 5 out of 7 models have precipitation anomalies of the same sign.

Acknowledgements. We appreciate the valuable comments and suggestions provided by the editor and anonymous reviewers, which greatly enhanced the quality of the manuscript. This work is supported by the National Key R&D Program of China (2022YFF0801602). We acknowledge the High-Performance Computing Center of Nanjing University of Information Science and Technology for their support of this work.

Data Availability Statement. The ERA5 dataset can be obtained from https://cds.climate.copernicus.eu/cdsapp#!/dataset/reanalysis-era5-single-levels-monthly-means?tab=form. HadISST data are available at https://www.metoffice.gov.uk/hadobs/hadisst/data/download.html.Monthly subsurface ocean temperature data is from https://cds.climate.copernicus.eu/cdsapp#!/dataset/reanalysis-oras5?tab=overview, CMAP precipitation data are derived from https://psl.noaa.gov/data/gridded/data.cmap.html.CMIP6 model data are available from the CMIP6 Search Interface at https://esgf-node.llnl.gov/search/cmip6.

Electronic supplementary material: Supplementary material is available in the online version of this article at https://doi.org/10.1007/s00376-023-3196-1.

REFERENCES

Alexander, M., and J. Scott, 2002: The influence of ENSO on air-sea interaction in the Atlantic. *Geophys. Res. Lett.*, **29**, 46-1–46-4, https://doi.org/10.1029/2001GL014347.

Ashok, K., S. K. Behera, S. A. Rao, H. Y. Weng, and T. Yamagata, 2007: El Niño Modoki and its possible teleconnection. *J. Geophys. Res.: Oceans*, **112**, C11007, https://doi.org/10.1029/2006JC003798.

Ashok, K., S. Iizuka, S. A. Rao, N. H. Saji, and W.-J. Lee, 2009: Processes and boreal summer impacts of the 2004 El Niño Modoki: An AGCM study. *Geophys. Res. Lett.*, **36**, L04703,

https://doi.org/10.1029/2008GL036313.

Bladé, I., M. Newman, M. A. Alexander, and J. D. Scott, 2008: The late fall extratropical response to ENSO: Sensitivity to coupling and convection in the tropical West Pacific. *J. Climate*, **21**, 6101–6118, https://doi.org/10.1175/2008JCLI1612.1.

Brönnimann, S., 2007: Impact of El Niño–Southern Oscillation on European climate. *Rev. Geophys.*, **45**, RG3003, https://doi.org/10.1029/2006RG000199.

Cai, W. J., and Coauthors, 2014: Increasing frequency of extreme El Niño events due to greenhouse warming. *Nature Climate Change*, **4**, 111–116, https://doi.org/10.1038/nclimate2100.

Chiodi, A. M., and D. E. Harrison, 2013: El Niño impacts on seasonal U.S. atmospheric circulation, temperature, and precipitation anomalies: The OLR-event perspective. *J. Climate*, **26**, 822–837, https://doi.org/10.1175/JCLI-D-12-00097.1.

Chiodi, A. M., and D. E. Harrison, 2015: Global seasonal precipitation anomalies robustly associated with El Niño and La Niña events—An OLR perspective. *J. Climate*, **28**, 6133–6159, https://doi.org/10.1175/JCLI-D-14-00387.1.

Duchon, C. E., 1979: Lanczos filtering in one and two dimensions. *Journal of Applied Meteorology and Climatology*, **18**, 1016–1022, https://doi.org/10.1175/1520-0450(1979)018<1016:LFIOAT>2.0.CO;2.

Eyring, V., S. Bony, G. A. Meehl, C. A. Senior, B. Stevens, R. J. Stouffer, and K. E. Taylor, 2016: Overview of the Coupled Model Intercomparison Project Phase 6 (CMIP6) experimental design and organization. *Geoscientific Model Development*, **9**, 1937–1958, https://doi.org/10.5194/gmd-9-1937-2016.

Feng, J., L. Wang, W. Chen, S. K. Fong, and K. C. Leong, 2010: Different impacts of two types of Pacific Ocean warming on Southeast Asian rainfall during boreal winter. *J. Geophys. Res.: Atmos.*, **115**, D24122, https://doi.org/10.1029/2010JD014761.

Geng, X., W. J. Zhang, M. F. Stuecker, and F.-F. Jin, 2017: Strong sub-seasonal wintertime cooling over East Asia and Northern Europe associated with super El Niño events. *Scientific Reports*, **7**, 3770, https://doi.org/10.1038/s41598-017-03977-2.

Geng, X., W. J. Zhang, Y. Y. Xiang, and F. Jiang, 2021: Dominant spatiotemporal variability of wintertime precipitation days in China and the linkage with large-scale climate drivers. *International Journal of Climatology*, **41**, 3561–3577, https://doi.org/10.1002/joc.7035.

Gill, E. C., B. Rajagopalan, and P. Molnar, 2015: Subseasonal variations in spatial signatures of ENSO on the Indian summer monsoon from 1901 to 2009. *J. Geophys. Res.: Atmos.*, **120**, 8165–8185, https://doi.org/10.1002/2015JD023184.

Guo, Z., T. J. Zhou, and B. Wu, 2017: The asymmetric effects of El Niño and La Niña on the East Asian winter monsoon and their simulation by CMIP5 atmospheric models. *J. Meteor. Res.*, **31**, 82–93, https://doi.org/10.1007/s13351-017-6095-5.

Harrison, D. E., and N. K. Larkin, 1996: The COADS sea level pressure signal: A near-global El Niño composite and time series view, 1946–1993. *J. Climate*, **9**, 3025–3055, https://doi.org/10.1175/1520-0442(1996)009<3025:TCSLPS>2.0.CO;2.

He, C., R. Liu, X. M. Wang, S. C. Liu, T. J. Zhou, and W. H. Liao, 2019: How does El Niño–Southern Oscillation modulate the interannual variability of winter haze days over eastern China. *Science of the Total Environment*, **651**, 1892–1902, https://doi.org/10.1016/j.scitotenv.2018.10.100.

Hersbach, H., and Coauthors, 2020: The ERA5 global reanalysis. *Quart. J. Roy. Meteor. Soc.*, **146**, 1999–2049, https://doi.org/10.1002/qj.3803.

Hoskins, B. J., and D. J. Karoly, 1981: The steady linear response of a spherical atmosphere to thermal and orographic forcing. *J. Atmos. Sci.*, **38**, 1179–1196, https://doi.org/10.1175/1520-0469(1981)038<1179:TSLROA>2.0.CO;2.

Hu, S. Q., W. J. Zhang, F. Jiang, and F.-F. Jin, 2023: Understanding the sub-seasonal variation in the wintertime AO spatial pattern from the viewpoint of El Niño–Southern Oscillation. *Climate Dyn.*, **60**, 3629–3643, https://doi.org/10.1007/s00382-022-06533-5.

Ineson, S., and A. A. Scaife, 2009: The role of the stratosphere in the European climate response to El Niño. *Nature Geoscience*, **2**, 32–36, https://doi.org/10.1038/ngeo381.

Jiang, F., W. J. Zhang, X. Geng, M. F. Stuecker, and C. Liu, 2019: Impacts of Central Pacific El Niño on Southern China spring precipitation controlled by its longitudinal position. *J. Climate*, **32**, 7823–7836, https://doi.org/10.1175/JCLI-D-19-0266.1.

Kao, H.-Y., and J.-Y. Yu, 2009: Contrasting Eastern-Pacific and Central-Pacific types of ENSO. *J. Climate*, **22**, 615–632, https://doi.org/10.1175/2008JCLI2309.1.

Kim, S., H.-Y. Son, and J.-S. Kug, 2018: Relative roles of equatorial central Pacific and western North Pacific precipitation anomalies in ENSO teleconnection over the North Pacific. *Climate Dyn.*, **51**, 4345–4355, https://doi.org/10.1007/s00382-017-3779-6.

Kirkland, E. J., 2010: Bilinear interpolation. *Advanced Computing in Electron Microscopy*, E. J. Kirkland, Ed., Springer, 261–263, https://doi.org/10.1007/978-1-4419-6533-2_12.

Kug, J.-S., F.-F. Jin, and S.-I. An, 2009: Two types of El Niño events: Cold tongue El Niño and warm pool El Niño. *J. Climate*, **22**, 1499–1515, https://doi.org/10.1175/2008JCLI2624.1.

Larkin, N. K., and D. E. Harrison, 2005: On the definition of El Niño and associated seasonal average U.S. weather anomalies. *Geophys. Res. Lett.*, **32**, D24122, https://doi.org/10.1029/2005GL022738.

Li, C., and H. Ma, 2012: Relationship between ENSO and winter rainfall over Southeast China and its decadal variability. *Adv. Atmos. Sci.*, **29**, 1129–1141, https://doi.org/10.1007/s00376-012-1248-z.

Li, J. N., D. Z. Huang, F. Z. Li, and Z. P. Wen, 2018: Circulation characteristics of EP and CP ENSO and their impacts on precipitation in South China. *Journal of Atmospheric and Solar-Terrestrial Physics*, **179**, 405–415, https://doi.org/10.1016/j.jastp.2018.09.006.

Livezey, R. E., M. Masutani, A. Leetmaa, H. L. Rui, M. Ji, and A. Kumar, 1997: Teleconnective response of the Pacific–North American region atmosphere to large central equatorial Pacific SST anomalies. *J. Climate*, **10**, 1787–1820, https://doi.org/10.1175/1520-0442(1997)010<1787:TROTPN>2.0.CO;2.

Ma, T. J., and Coauthors, 2022: Different ENSO teleconnections over East Asia in early and late winter: Role of precipitation anomalies in the tropical Indian Ocean and far western

Pacific. *J. Climate*, **35**, 7919–7935, https://doi.org/10.1175/JCLI-D-21-0805.1.

Mariotti, A., N. Zeng, and K.-M. Lau, 2002: Euro-Mediterranean rainfall and ENSO—a seasonally varying relationship. *Geophys. Res. Lett.*, **29**, 59-1–59-4, https://doi.org/10.1029/2001GL014248.

McPhaden, M. J., S. E. Zebiak, and M. H. Glantz, 2006: ENSO as an integrating concept in earth science. *Science*, **314**, 1740–1745, https://doi.org/10.1126/science.1132588.

Moron, V., and I. Gouirand, 2003: Seasonal modulation of the El Niño–Southern Oscillation relationship with sea level pressure anomalies over the North Atlantic in October–March 1873–1996. *International Journal of Climatology*, **23**, 143–155, https://doi.org/10.1002/joc.868.

Park, C.-H., J. Choi, S.-W. Son, D. Kim, S.-W. Yeh, and J.-S. Kug, 2023: Sub-seasonal variability of ENSO teleconnections in western North America and its prediction skill. *J. Geophys. Res.: Atmos.*, **128**, e2022JD037985, https://doi.org/10.1029/2022JD037985.

Rayner, N. A., D. E. Parker, E. B. Horton, C. K. Folland, L. V. Alexander, D. P. Rowell, E. C. Kent, and A. Kaplan, 2003: Global analyses of sea surface temperature, sea ice, and night marine air temperature since the late nineteenth century. *J. Geophys. Res.: Atmos.*, **108**, 4407, https://doi.org/10.1029/2002JD002670.

Ren, H.-L., and F.-F. Jin, 2011: Niño indices for two types of ENSO. *Geophys. Res. Lett.*, **38**, L04704, https://doi.org/10.1029/2010GL046031.

Ropelewski, C. F., and M. S. Halpert, 1987: Global and regional scale precipitation patterns associated with the El Niño/Southern Oscillation. *Mon. Wea. Rev.*, **115**, 1606–1626, https://doi.org/10.1175/1520-0493(1987)115<1606:GARSPP>2.0.CO;2.

Son, H.-Y., J.-Y. Park, J.-S. Kug, J. Yoo, and C.-H. Kim, 2014: Winter precipitation variability over Korean Peninsula associated with ENSO. *Climate Dyn.*, **42**, 3171–3186, https://doi.org/10.1007/s00382-013-2008-1.

Su, J.-Z., R.-H. Zhang, and C.-W. Zhu, 2013: ECHAM5-simulated impacts of two types of El Niño on the winter precipitation anomalies in South China. *Atmospheric and Oceanic Science Letters*, **6**, 360–364, https://doi.org/10.3878/j.issn.1674-2834.13.0013.

Su, J. Z., R. H. Zhang, T. M. Li, X. Y. Rong, J.-S. Kug, and C.-C. Hong, 2010: Causes of the El Niño and La Niña amplitude asymmetry in the equatorial eastern Pacific. *J. Climate*, **23**, 605–617, https://doi.org/10.1175/2009JCLI2894.1.

Trenberth, K. E., and J. M. Caron, 2000: The Southern Oscillation revisited: Sea level pressures, surface temperatures, and precipitation. *J. Climate*, **13**, 4358–4365, https://doi.org/10.1175/1520-0442(2000)013<4358:TSORSL>2.0.CO;2.

Wallace, J. M., and D. S. Gutzler, 1981: Teleconnections in the geopotential height field during the northern hemisphere winter. *Mon. Wea. Rev.*, **109**, 784–812, https://doi.org/10.1175/1520-0493(1981)109<0784:TITGHF>2.0.CO;2.

Wallace, J. M., E. M. Rasmusson, T. P. Mitchell, V. E. Kousky, E. S. Sarachik, and H. von Storch, 1998: On the structure and evolution of ENSO-related climate variability in the tropical Pacific: Lessons from TOGA. *J. Geophys. Res.: Oceans*, **103**, 14241–14259, https://doi.org/10.1029/97JC02905.

Wang, B., R. G. Wu, and X. H. Fu, 2000: Pacific-East Asian teleconnection: How does ENSO affect East Asian climate?. *J. Climate*, **13**, 1517–1536, https://doi.org/10.1175/1520-0442(2000)013<1517:PEATHD>2.0.CO;2.

Weng, H. Y., K. Ashok, S. K. Behera, S. A. Rao, and T. Yamagata, 2007: Impacts of recent El Niño Modoki on dry/wet conditions in the Pacific rim during boreal summer. *Climate Dyn.*, **29**, 113–129, https://doi.org/10.1007/s00382-007-0234-0.

Wu, B., T. M. Li, and T. J. Zhou, 2010: Asymmetry of atmospheric circulation anomalies over the western North Pacific between El Niño and La Niña. *J. Climate*, **23**, 4807–4822, https://doi.org/10.1175/2010JCLI3222.1.

Wu, R. G., Z.-Z. Hu, and B. P. Kirtman, 2003: Evolution of ENSO-related rainfall anomalies in East Asia. *J. Climate*, **16**, 3742–3758, https://doi.org/10.1175/1520-0442(2003)016<3742:EOERAI>2.0.CO;2.

Xie, P. P., and P. A. Arkin, 1997: Global precipitation: A 17-year monthly analysis based on gauge observations, satellite estimates, and numerical model outputs. *Bull. Amer. Meteor. Soc.*, **78**, 2539–2558, https://doi.org/10.1175/1520-0477(1997)078<2539:GPAYMA>2.0.CO;2.

Xie, S.-P., K. M. Hu, J. Hafner, H. Tokinaga, Y. Du, G. Huang, and T. Sampe, 2009: Indian Ocean capacitor effect on Indo–western Pacific climate during the summer following El Niño. *J. Climate*, **22**, 730–747, https://doi.org/10.1175/2008JCLI2544.1.

Xu, K., Q.-L. Huang, C.-Y. Tam, W. Q. Wang, S. Chen, and C. W. Zhu, 2019: Roles of tropical SST patterns during two types of ENSO in modulating wintertime rainfall over southern China. *Climate Dyn.*, **52**, 523–538, https://doi.org/10.1007/s00382-018-4170-y.

Yang, J. L., Q. Y. Liu, S.-P. Xie, Z. Y. Liu, and L. X. Wu, 2007: Impact of the Indian Ocean SST basin mode on the Asian summer monsoon. *Geophys. Res. Lett.*, **34**, L02708, https://doi.org/10.1029/2006GL028571.

Yin, Z. C., and H. J. Wang, 2016: The relationship between the subtropical Western Pacific SST and haze over North-Central North China Plain. *International Journal of Climatology*, **36**, 3479–3491, https://doi.org/10.1002/joc.4570.

Yuan, Y., and S. Yang, 2012: Impacts of different types of El Niño on the East Asian climate: Focus on ENSO cycles. *J. Climate*, **25**, 7702–7722, https://doi.org/10.1175/JCLI-D-11-00576.1.

Zhang, R. H., and A. Sumi, 2002: Moisture circulation over East Asia during El Niño episode in northern winter, spring and autumn. *J. Meteor. Soc. Japan*, **80**, 213–227, https://doi.org/10.2151/jmsj.80.213.

Zhang, R. H., A. Sumi, and M. Kimoto, 1996: Impact of El Niño on the East Asian monsoon: A diagnostic study of the '86/87 and '91/92 events. *J. Meteor. Soc. Japan*, **74**, 49–62, https://doi.org/10.2151/jmsj1965.74.1_49.

Zhang, R. H., Q. Y. Min, and J. Z. Su, 2017: Impact of El Niño on atmospheric circulations over East Asia and rainfall in China: Role of the anomalous western North Pacific anticyclone. *Science China Earth Sciences*, **60**, 1124–1132, https://doi.org/10.1007/s11430-016-9026-x.

Zhang, R. H., T. R. Li, M. Wen, and L. K. Liu, 2015a: Role of intraseasonal oscillation in asymmetric impacts of El Niño and La Niña on the rainfall over southern China in boreal winter. *Climate Dyn.*, **45**, 559–567, https://doi.org/10.1007/

s00382-014-2207-4.

Zhang, W. J., H. Y. Li, M. F. Stuecker, F.-F. Jin, and A. G. Turner, 2016: A new understanding of El Niño's impact over East Asia: Dominance of the ENSO combination mode. *J. Climate*, **29**, 4347–4359, https://doi.org/10.1175/JCLI-D-15-0104.1.

Zhang, W. J., H. Y. Li, F.-F. Jin, M. F. Stuecker, A. G. Turner, and N. P. Klingaman, 2015b: The annual-cycle modulation of meridional asymmetry in ENSO's atmospheric response and its dependence on ENSO zonal structure. *J. Climate*, **28**, 5795–5812, https://doi.org/10.1175/JCLI-D-14-00724.1.

Zhou, L.-T., and R. G. Wu, 2010: Respective impacts of the East Asian winter monsoon and ENSO on winter rainfall in China. *J. Geophys. Res.: Atmos*, **115**, D02107, https://doi.org/10.1029/2009JD012502.